Tritium gas flow dynamics through the source and transport system of the Karlsruhe tritium neutrino experiment

O. B. Malyshev, Chr. Day, X. Luo, and F. Sharipov

Citation: Journal of Vacuum Science & Technology A **27**, 73 (2009); doi: 10.1116/1.3039679
View online: https://doi.org/10.1116/1.3039679
View Table of Contents: https://avs.scitation.org/toc/jva/27/1
Published by the American Vacuum Society

ARTICLES YOU MAY BE INTERESTED IN

Introduction to MOLFLOW+: New graphical processing unit-based Monte Carlo code for simulating molecular flows and for calculating angular coefficients in the compute unified device architecture environment
Journal of Vacuum Science & Technology A **27**, 1017 (2009); https://doi.org/10.1116/1.3153280

Data on Internal Rarefied Gas Flows
Journal of Physical and Chemical Reference Data **27**, 657 (1998); https://doi.org/10.1063/1.556019

Rarefied gas flow through a long tube at any temperature ratio
Journal of Vacuum Science & Technology A **14**, 2627 (1996); https://doi.org/10.1116/1.579991

Rarefied gas flow through a long tube at arbitrary pressure and temperature drops
Journal of Vacuum Science & Technology A **15**, 2434 (1997); https://doi.org/10.1116/1.580904

Separation phenomena for gaseous mixture flowing through a long tube into vacuum
Physics of Fluids **17**, 127102 (2005); https://doi.org/10.1063/1.2140290

Gaseous mixture flow through a long tube at arbitrary Knudsen numbers
Journal of Vacuum Science & Technology A **20**, 814 (2002); https://doi.org/10.1116/1.1469010

HIDEN ANALYTICAL
Instruments for **Advanced Science**
Contact Hiden Analytical for further details:
W www.HidenAnalytical.com
E info@hiden.co.uk
CLICK TO VIEW our product catalogue
Gas Analysis
- dynamic measurement of reaction gas streams
- catalysis and thermal analysis
- molecular beam studies
- dissolved species probes
- fermentation, environmental and ecological studies

Surface Science
- UHV TPD
- SIMS
- end point detection in ion beam etch
- elemental imaging - surface mapping

Plasma Diagnostics
- plasma source characterization
- etch and deposition process reaction kinetic studies
- analysis of neutral and radical species

Vacuum Analysis
- partial pressure measurement and control of process gases
- reactive sputter process control
- vacuum diagnostics
- vacuum coating process monitoring

Tritium gas flow dynamics through the source and transport system of the Karlsruhe tritium neutrino experiment

O. B. Malyshev[a)]
ASTeC, STFC Daresbury Laboratory, Warrington, Cheshire WA4 4AD, United Kingdom

Chr. Day and X. Luo
Forschungszentrum Karlsruhe, Institute for Technical Physics, P.O. Box 3640, 76021 Karlsruhe, Germany

F. Sharipov
Departamento de Física, Universidade Federal do Paraná, Caixa Postal 19044, Curitiba 81531-900, Brazil

(Received 12 November 2007; accepted 3 November 2008; published 30 December 2008)

The source and transport system of the Karlsruhe tritium neutrino experiment (KATRIN) must provide a significant reduction in tritium flow and gas density. It comprises a 10 m long windowless source tube, where the tritium gas is injected, followed by a differential pumping system and a cryogenic pumping system. The primary challenge of the analysis is that the gas flow changes from a viscous flow regime inside the source tube to a transitional flow regime at the first pumping stage, and to a molecular flow regime at the remaining stages of the differential pumping system and further downstream. A strong molecular beaming effect must be considered. This article presents the results of calculations of gas density and flow for the complete source and differential pumping system. It is shown that a total flow-rate reduction factor of 1.4×10^{-8} can be attained, which is one of the prerequisites to achieve extreme-high vacuum conditions in the spectrometers used in the downstream end of the experiment. © *2009 American Vacuum Society.* [DOI: 10.1116/1.3039679]

I. INTRODUCTION

The Karlsruhe tritium neutrino experiment (KATRIN) is a large vacuum system that aims to measure the mass of the electron antineutrino from the β-decay of tritium with unprecedented sensitivity.[1,2] To achieve this goal, the injected tritium gas flow must be significantly reduced along the beamline by means of a modular differential pumping system. An international collaboration will construct and operate the experiment in the European Tritium Laboratory on the site of Forschungszentrum Karlsruhe. A detailed description of the KATRIN vacuum system, its requirements, and challenges can be found in Ref. 2.

The KATRIN vacuum system has an overall length of about 70 m, comprising four main parts: a gaseous tritium source, a transport section, a system of two electrostatic filters (pre- and main spectrometer), and the electron detector; Fig. 1 shows an overall layout of KATRIN. In the center there is the windowless gaseous tritium source (WGTS) that must provide a given strength of the decay signal. To achieve this, a cross-section-related molecular column density of $N=0.5\times10^{22}$ m^{-2} at the temperature $T=27$ K must be maintained in the 10 m long source tube. This is achieved by a continuous tritium inlet gas flow in the middle and by continuous tritium pumping at its ends. The required column density corresponds to a continuous tritium throughput of approximately 1.8 mbar l/s (referred to the temperature 273.15 K) at an injection pressure of about 3×10^{-3} mbar. This density defines the production rate of the electrons and antineutrinos, which is given by the number of tritium molecules contained in the source tube volume. The WGTS is symmetric and features two identical differential pumping systems (DPS), one at each side. The one in the rear direction (see Fig. 2) will reduce the tritium flow to a rear system containing an electron gun used for system calibration. The other system in the forward direction has two differential pumping systems DPS1-F and DPS2-F (see Figs. 1 and 2) and a cryogenic pumping system (CPS) designed to reduce the tritium flow significantly. These pumping systems are surrounded by sophisticated superconducting magnets to transport adiabatically the decay electrons (β-particles) to the spectrometers.[3] To achieve the unprecedented sensitivity of 0.2 eV, a pressure below 10^{-11} mbar will be required in the electrostatic tandem spectrometer, with a negligible tritium partial pressure (on the order of 10^{-20} mbar).

II. FLOW-RATE REDUCTION FACTOR REQUIREMENTS

The prime objective of the KATRIN beamline vacuum pumping system is to provide a significant reduction in the tritium flow rate. On the other hand, the beamline must be kept as short as possible due to operational constraints; because the beamline is operated under cryogenic conditions and the β-particles are guided via superconducting magnets, this has major cost implications. In order to optimize the design, one must develop a model of the gas flow dynamics through the source and transport system, such that the number of pumping stages, the number of pumps, their pumping speed, as well as other parameters can be varied and its influence on the overall flow-rate reduction can be studied. This article therefore presents a complete description of the beamline in terms of flow rates and density.

a)Electronic mail: oleg.malyshev@stfc.ac.uk

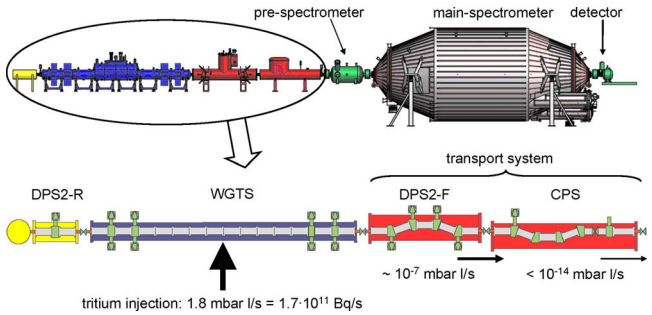


FIG. 1. (Color online) KATRIN layout.

Based on the symmetry of the WGTS (see Fig. 1), it can be assumed that 50% of the injected gas throughput is directed into the forward direction of the beamline, about 1 mbar l/s. Then there are two downstream limitations to meet:

(1) The maximum allowed tritium flow into CPS is 1 Ci/60 days due to safety regulation reasons, equal to 8×10^{-8} mbar l/s. This leads to the required flow-rate reduction factor K greater than 1.4×10^{-8} for the complete differential pumping section (DPS1-F and DPS2-F).

(2) For the KATRIN experiment, it is crucial that the spectrometers are kept essentially free of tritium. The maximum allowed tritium flow rate into the main spectrometer is defined by the experimental background caused by the decay of tritium molecules in the main spectrometer and will be a maximum of 10^{-3} counts/s (which gives a residual tritium partial pressure in the main spectrometer of $P_{MS} < 10^{-20}$ mbar). It has been estimated that a tritium flow rate of $\sim 10^{-14}$ mbar l/s into the prespectrometer will ensure an acceptably low background increase in the main spectrometer.[2] This leads to the required flow-rate reduction factor K from source to spectrometer inlet of approximately 10^{-14}.

III. MODELING OF WGTS AND DIFFERENTIAL PUMPING SYSTEM

The difficulty of the analysis is that the gas flow changes from a viscous flow regime inside WGTS to a transitional flow regime at the first pumping stage, and finally to a molecular flow regime throughout the remaining part of the transport system. The flow regime of rarefied gases is described by the Knudsen number Kn, which is defined as the ratio of the molecular mean free path and the tube radius, or by the rarefaction parameter δ, which is proportional to the inverse Knudsen number. The transitional regime is characterized by values of $\mathrm{Kn} \sim 1$ or $\delta \sim 1$. At the injection point of the WGTS tube (tritium, 27 K, $d=90$ mm), a rarefaction parameter is $\delta=20$, which clearly indicates a viscous regime. At the exit point, the rarefaction parameter is small ($\delta \ll 1$), i.e., the gas flow is free molecular.

For simple geometries such as the source tube, the kinetic Boltzmann equation can be solved for the whole range of gas rarefaction. However, outside the tube, the geometry of the system is very complicated and another method must be used. One of the commonly chosen methods is the diffusion model. However preliminary analyses have shown that in the case of the molecular gas flow regime, there is a strong molecular beaming effect. Therefore, one-dimensional diffusion models lead to significant errors and should not be used, and three-dimensional modeling must be applied instead. This is why we are using the test particle Monte Carlo method, which is quite appropriate for free-molecular flows through complicated geometrical systems.

Another problem related to the use of numerical methods: the calculations should be completed within a reasonable time, but the calculation time increases with the number of test particles, complexity of the model, and ratio between largest and smallest size of the model. In addition, for the KATRIN transport system, characterized by a required flow-

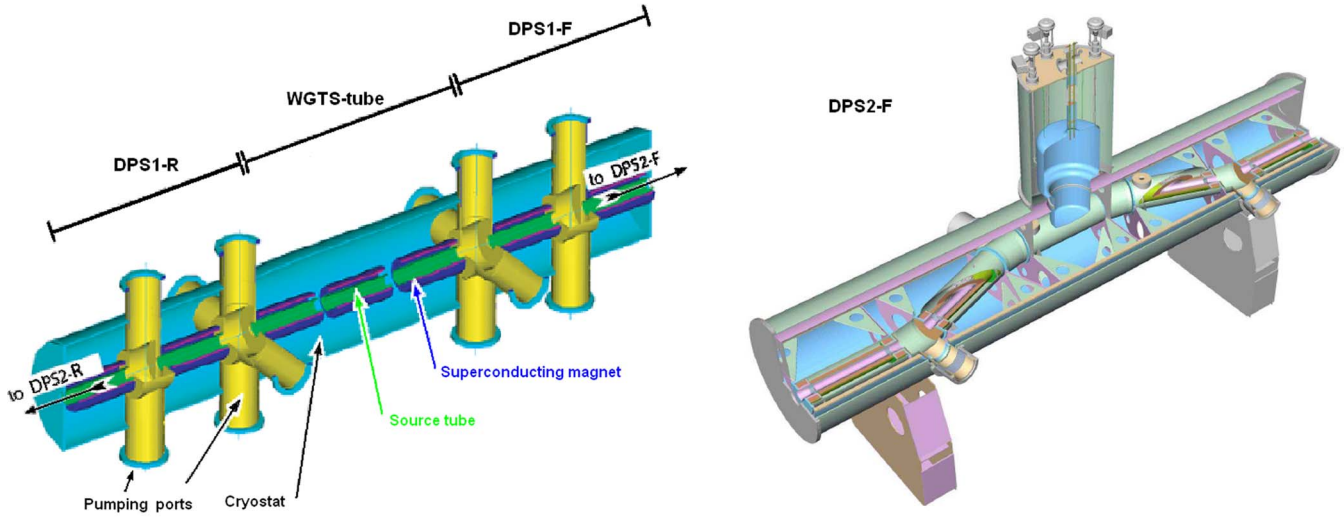


FIG. 2. (Color online) WGTS with DPS1-F and DPS2-F layouts.

rate reduction factor in the order of $K \approx 10^{-14}$, one needs to generate at least $\sim 10^{16}$ test particles to obtain the modeling result with reasonably good statistics for accuracy of $\sim 10\%$. This will require unacceptably long computing time.

To overcome these difficulties, the transport system was first analyzed element by element. For that purpose, the KATRIN gas flow model was divided according to the real KATRIN hardware sections: WGTS tube, DPS1-F, DPS2-F, and CPS (see Figs. 1 and 2). In the second step, additional analysis was performed to merge the individual results.

A. WGTS tube

The WGTS is a tube having a length $L=10$ m and radius $R=45$ mm. Tritium is injected in the middle cross section of the tube through many small holes, and it then flows to the tube ends where it is pumped by the vacuum systems. The main difficulty of this calculation is that the regime of flow is hydrodynamic in the injection point and transitional or practically free molecular at the source ends. Under such conditions, the problem can be solved only by the kinetic Boltzmann equation.

To characterize the gas rarefaction, the following parameter δ is introduced:

$$\delta = \frac{PR}{\mu v_m}, \quad v_m = \left(\frac{2R_g T}{m}\right)^{1/2}, \tag{1}$$

where P is the pressure, μ is the gaseous shear viscosity, v_m is the most-probable molecular speed, R_g is the gaseous constant, and m is the molecular mass. The throughput q is expressed via the reduced flow rate G_P as

$$q = \frac{R_g T_0}{m}\frac{\pi R^3}{v_m} G_P(\delta)\frac{dP}{dx}, \tag{2}$$

where $T_0=273.15$ K and x is the longitudinal coordinate with the origin at the middle tube section. The reduced flow rate G_P is the function of the local rarefaction parameter δ. The technique of calculation of G_P based on the kinetic equation is described in detail in Refs. 4–6, where the tube length is assumed to be significantly larger than its radius. In the problem in question, the length-to-radius ratio L/R is about 200, i.e., the above mentioned assumption is fulfilled.

Once the function $G_P(\delta)$ is known, Eq. (2) can be integrated along the tube from the middle section ($x=0$) to the tube end ($x=L/2$). As a result, we obtain

$$q = \frac{R_g T_0}{m}\frac{\pi R^3}{v_m} G(\delta_{ex}, \delta_{in})\frac{P_{in} - P_{ex}}{L/2}, \tag{3}$$

where the quantity $G(\delta_{ex}, \delta_{in})$ is determined by the rarefaction parameter at the source exit δ_{ex} and by that at the injection point δ_{in}. It is calculated via the flow rate G_P as

$$G = \frac{1}{\delta_{in} - \delta_{ex}} \int_{\delta_{ex}}^{\delta_{in}} G_P(\delta) d\delta. \tag{4}$$

To obtain Eqs. (3) and (4), relation (1) of the rarefaction parameter to the pressure has been used. In Ref. 4, it was shown that the relation

$$G(\delta_{ex}, \delta_{in}) = G_P\left(\frac{\delta_{ex} + \delta_{in}}{2}\right) \tag{5}$$

approximates very well the exact integration (4).

Our principal aim is to calculate the throughput q and the injection pressure P_{in} for a given column density N of the WGTS tube, defined as

$$N = \int_{-L/2}^{L/2} n(x) dx, \tag{6}$$

where $n(x)$ is the local number density of tritium, which can be calculated from Eq. (2). If one integrates this equation from the middle section ($x=0$) to an arbitrary cross section with the coordinate x, one obtains

$$q = R_g T_0 \pi R^3 v_m \frac{(n_{in} - n)}{2x} G_P\left(\frac{\delta_{in} + \delta}{2}\right). \tag{7}$$

Combining this equation with Eq. (3), we obtain

$$\frac{2x}{L} = \frac{n_{in} - n}{n_{in} - n_{ex}} \frac{G_P\left(\frac{\delta_{in} + \delta}{2}\right)}{G_P\left(\frac{\delta_{in} + \delta_{ex}}{2}\right)}. \tag{8}$$

So, in practice, one calculates the function $x=x(n)$. Then, this function is inverted and the column density is calculated by Eq. (6). Thus, it is necessary to fit P_{in} so that the column density is equal to the required value, i.e., $N=0.5 \times 10^{22}$ m^{-2}. Then, the throughput is calculated from Eq. (3).

To calculate the rarefaction parameter δ, some experimental data on the viscosity of tritium are necessary. Unfortunately, no data on the viscosity at low temperature are available in open literature. Some data on the viscosity of hydrogen and deuterium at low temperature are reported in Refs. 7–9. So, the viscosity of tritium μ_T can be calculated via the viscosity of deuterium μ_D assuming that both molecules have the same cross sections. In this case, we obtain $\mu_T = \sqrt{3/2}\mu_D$. This relation works very well for high temperature, when the rotations of both molecules T_2 and D_2 are classical. At low temperature, every molecule has its own spectrum of rotational energy, which affects the cross section. An analysis of the experimental data on hydrogen[7] and deuterium[8] showed that the analogous expression $\mu_D = \sqrt{2}\mu_H$ provides an overstated value of the viscosity μ_D by 7%. So, it is expected that such a relation provides the slightly overstated values of μ_T. The discrepancy should be within 5%. Finally, using the experimental value of $\mu_D = 2.084 \times 10^{-6}$ Pa s at $T=30$ K reported in Ref. 8, we obtain the viscosity of tritium as $\mu_T = 0.95\sqrt{3/2}\mu_D = 2.425 \times 10^{-6}$ Pa s. This value was used in our numerical calculations.

First, the calculations were carried out for the gas flow into vacuum, i.e., when $\delta_{ex}=0$. The density distribution in this case is shown on Fig. 3. However, in practice, the exit pressure P_{ex} is not so low to assume $\delta_{ex}=0$. Thus, additional calculations were carried out to study the influence of P_{ex} on the column density and throughput. The results of these cal-

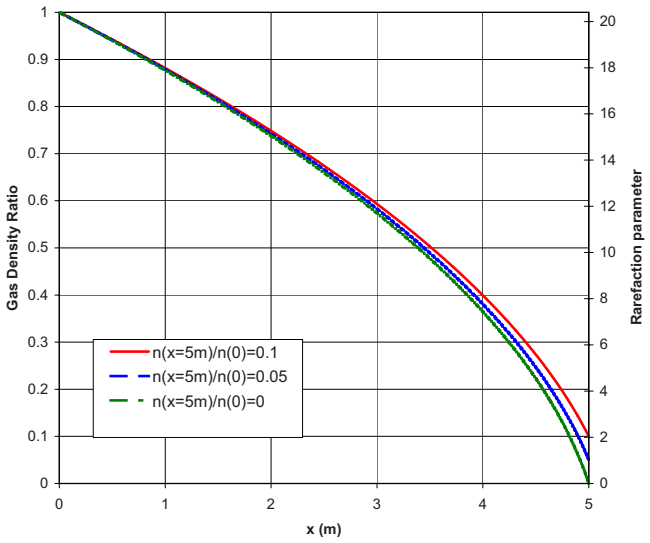


FIG. 3. (Color online) Tritium gas density ratio along WGTS tube.

culations are presented in Table I, which show that the influence is significant. In the future, when the pressure P_{ex} is measured, other calculations will be carried out for the measured values.

The present calculations were carried out assuming the complete accommodation of tritium on the tube wall. No data can be found about the accommodation coefficient of this gas at low temperature. In the Ref. 10 work, the accommodation coefficient of hydrogen on a glass surface at room temperature was calculated from experimental data on the slip coefficient. The obtained value is 0.952. It is difficult to say if tritium has a lower or higher accommodation coefficient at the low temperature, i.e., at $T=27$ K. It can simply be stated that it can vary in the range from 0.8 to 1. On the other hand, its influence on the flow rate is significant only in the free-molecular regime. To evaluate the influence of the accommodation coefficient on the column density N, some additional calculations were carried out for its value equal to 0.8, which showed that the uncertainty of the accommodation coefficient of 20% causes an uncertainty of the column density N within 1.6%. Thus, the calculations based on the diffuse gas-surface interaction are quite reliable.

B. Modeling of DPS2-F

In assessing the KATRIN vacuum pumping system, we started with the model of DPS2-F because it was clear that the gas flow regime is molecular and the available test particle Monte Carlo (TPMC) codes can be used without concern about intermolecular collisions. The detailed description of the model, assumptions, and the analysis of results of modeling were published in Ref. 11. It has been shown that by using the candidate turbomolecular pump (TMP), characterized by an effective capture probability at the pumping port of $\alpha_{TMP}=0.3$, a tritium flow-rate reduction factor of the complete DPS2-F system of about $K_{II}=1/(1.3\times10^5)=7.7\times10^{-6}$ can be achieved. Under these conditions, the calculated gas density ratio over the complete DPS2-F system was $R_{II}=1/(6.6\times10^6)=1.5\times10^{-7}$. It is necessary to mention that an accident case was also modeled: if one of TMPs connected to DPS2-F failed, the tritium flow-rate reduction factor K_{II}^* of the complete DPS2-F system will be about 30 times larger: $K_{II}^*=2.3\times10^{-4}$.

TABLE I. Column density N and throughput q vs exit pressure P_{ex} at $P_{in}=3.006$ bar.

P_{ex}/P_{in}	$N/10^{22}$ (1/m^2)	q (mbar 1/s at 0 °C)
0	0.5	1.853
0.005	0.5007	1.851
0.01	0.5014	1.848
0.05	0.5007	1.824
0.1	0.5167	1.788

C. Modeling of DPS1-F

From the modeling aspect, DPS1-F is the most challenging part of the transport section. There are transitional flow conditions at the inlet and free-molecular flow conditions in the outlet. Unfortunately, no solutions of the kinetic equation exist for such a complex geometry of pumping ports.

To accurately represent the flow situation, the direct-simulation Monte Carlo approach would be most appropriate. However, such work would be a very major effort and is not reasonable to do within an ongoing design process. This is why it was decided to use the conventional TPMC method, being aware that the final results might lead to lower reduction factors because the intermolecular collisions that are neglected in TPMC will reduce the molecular beaming effect; therefore the TPMC results might introduce some additional safety margin in the overall design and does not play any negative role.

Two DPS1 Monte Carlo models were built based on the design made by ACCEL Instruments GmbH. The core model includes the following elements (see Fig. 4):

- an inlet surface with sticking probability α_1 (ring 1 in Fig. 4);
- a part of WGTS (a 0.9 m long tube with a diameter of 90 mm that begins at $x=4$ m with respect to $x=0$ at the middle of WGTS), the tube ended by a cone (x is the axial coordinate);
- pumping port 1 with four ducts leading to TMP, four pumping surfaces (rings 2–5) with a capture probability α_{TMP}. The pumping port is of cubical shape with dimensions of $374\times374\times250$ mm^3; the pumping ducts are 656 mm in length and 250 mm in diameter;
- a tube between two pumping ports with cones at either side (1060 mm long, 90 mm diameter);
- pumping port 2 (of the same dimension as above) with two ducts leading to TMP, two pumping surface rings 6 and 7 with a capture probability α_{TMP}; the pumping ducts are 406 mm in length and 250 mm in diameter;
- a tube between the pumping port 2 and the gate valve in front of DPS2, with cones at either side (1060 mm long, 90 mm diameter);

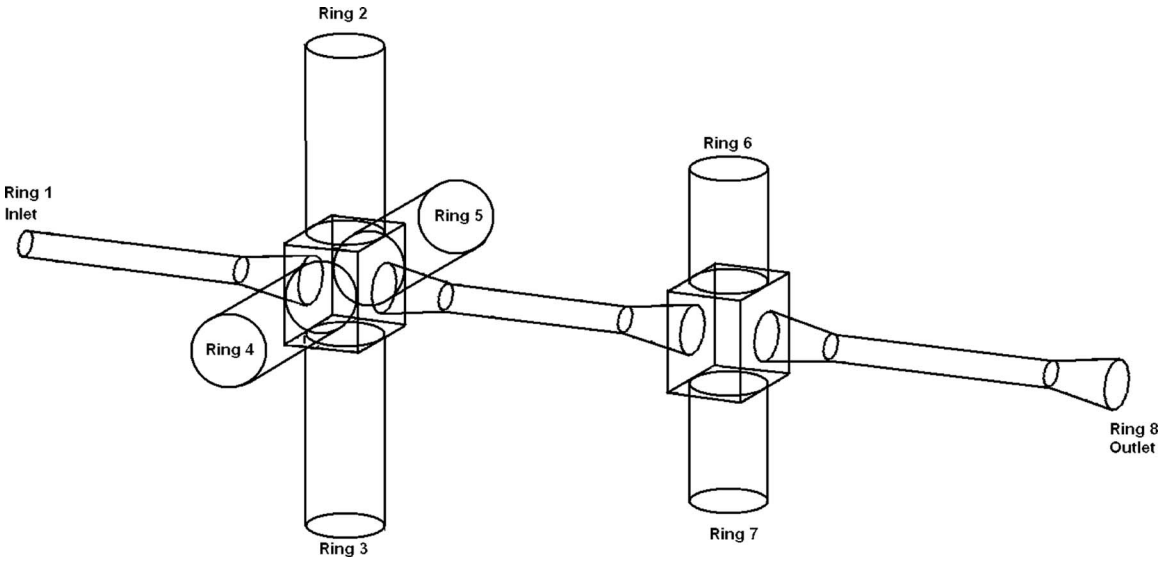


FIG. 4. Layout of the core model for DPS1.

- an outlet surface ring 8 with sticking probability α_N;
- in addition, Monte Carlo codes allow setting the few transparent test facets for gas density profile calculations. The test facets were set along the main axes and along one pumping duct at each pumping port.

The model contains one inlet surface ($i=1$), and seven outlet surfaces (four pumps in the first port, two pumps in the second port, and the outlet surface; $i=2,\ldots,8$). Two different Monte Carlo codes have been used[12,13] and no particular deviations were found.

Monte Carlo simulations have been performed the same way as described in Ref. 11, when the pumping surfaces (inlet, outlet, and pumping surface in pumping ducts) have a sticking probability of 1 and the particles were generated from one of the pumping surfaces. This was repeated four times, i.e., for the inlet, pumping port 1, pumping port 2, and the outlet. The number of generated particles was 10^7 for each run. Results of the modeling were as follows:

- the transmission probability matrix **W** and
- a number of particles m_j passed through each of 200 elements along the test facets.

1. Flow-rate reduction factor and gas density ratio as a function of the pump capture probability

Following the procedure described in Ref. 11, a vector **f** of the incoming flow f_i to each pumping surface can be found by solving the matrix equation with the transmission probability matrix **W** for a vector **f**,

$$[\mathbf{E}-\mathbf{W}\ \mathrm{diag}(1-\mathbf{a})]\cdot\mathbf{f}=\mathbf{W}\cdot\mathbf{d}, \tag{9}$$

where **E** is a unit matrix, **W** is the transmission probability matrix, $\mathrm{diag}(1-\alpha)$ is the diagonal matrix of vector $(1-\alpha)$, where α is a vector of capture probability, and **d** is the gas desorption (or injection) vector. In the case of DPS1, tritium comes from the inlet surface only: $d_1>0$ and $d_i=0$ for $i=2,\ldots,8$. The sticking probability vector was defined as the following: $\alpha_1=0$ (inlet surface), $\alpha_i=0.3$ for $i=2,\ldots,7$ (TMPs), the capture probability of the outlet surface α_N must be equal to the downstream section capture probability $\chi_{\mathrm{DPS2\text{-}F}}$. The later was evaluated with the Monte Carlo results for DPS2-F (Ref. 11) and formula (15) below as $\chi_{\mathrm{DPS2\text{-}F}}=0.078$; therefore, $\alpha_{\mathrm{N\ DPS1\text{-}F}}=0.078$.

Having the solutions for **f**, the gas flows **Q** at every boundary surfaces can be calculated from Eq. (5). The overall efficiency of DPS1-F is characterized by the flow-rate reduction factor K_I as the ratio of fluxes at the outlet and inlet of DPS1-F. The efficiency of the differential pumping at the first pumping port with four TMPs and at the second pumping port with two TMPs can be characterized by the individual flow-rate reduction factors K_{Ia} and K_{Ib}, i.e., the ratio of fluxes after and before the pumping ports, as follows:

$$K_I=\frac{\alpha_N f_N}{1-\alpha_1 f_1},\quad K_{Ia}=\frac{\Sigma_{j=6}^{N}\alpha_i f_i}{1-\alpha_1 f_1},\quad K_{Ib}=\frac{\alpha_N f_N}{\Sigma_{j=6}^{N}\alpha_i f_i}. \tag{10}$$

Figure 5 presents the individual pump port flow-rate reduction factors, together with the overall value K_I. One can see that assuming the pump capture probability of 0.3, based on the results in Ref. 4, the gas flow is reduced ~30 times after the pumping port 1 and ~10 times after the pumping port 2; the total flow-rate reduction factor is $K_I\approx 0.003$.

The *gas density ratio* R_i, which is defined as the ratio of the gas density at inlet surface and surface i, can be estimated as

$$R_i=\frac{n_1}{n_i}=\frac{d_1+(2-\alpha_1)f_1}{(2-\alpha_i)f_i}\frac{A_i}{A_0},\quad i=2,\ldots,8, \tag{11}$$

where the A_i are the cross-sectional areas of corresponding boundary surfaces.

In fact, these two ratios (K_i and R_i) do not depend on α_1 because by changing α_1, one changes the injected flow Q_1 but does not change the transmission probabilities between

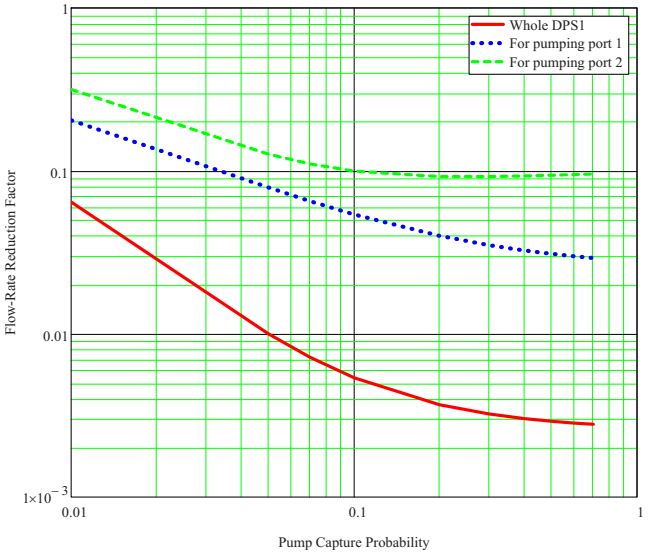


FIG. 5. (Color online) DPS1 gas flow-rate reduction factor as a function of turbomolecular pump capture probability.

surfaces. Therefore, the fraction of injected flow pumped by each pump does not depend on the absolute value of this flow (remaining within molecular flow regime). The same considerations are valid for the gas density ratio. Meanwhile, both ratios depend on the sticking probability of outlet surface.

The overall gas density ratio R_I (the ratio of the gas density at the DPS1 outlet and inlet) is shown in Fig. 6, together with the gas flow-rate reduction factor. One can see that both the gas density ratio and flow-rate reduction factor are quite sensitive to the pump capture probability less than 0.2–0.3. For the higher capture probability, this dependence is quite small. That means that the conductance (or transmission probability) of the pumping ducts is a limiting factor for the gas density ratio and flow-rate reduction factor.

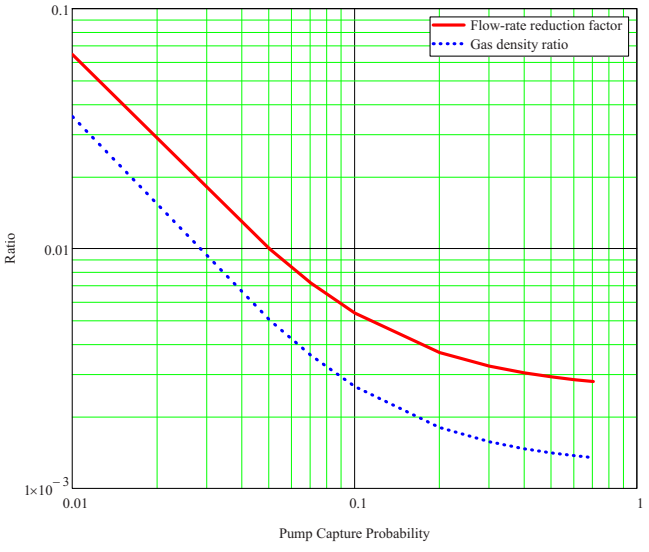


FIG. 6. (Color online) DPS1 gas flow-rate reduction factor and density ratio as a function of turbomolecular pump capture probability.

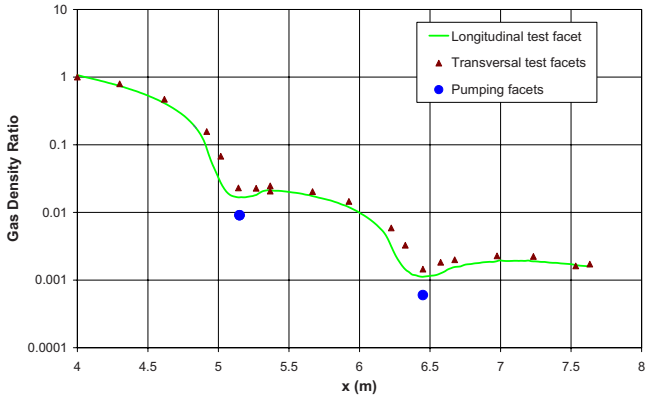


FIG. 7. (Color online) Gas density ratio along DPS1 and at the pumping ports.

2. Gas density ratio along the DPS1

The MOLFLOW code allows setting a transparent test strip consisting of 100 pieces to count the number of particles passing through it. This can then be converted into the gas density profile. In general, this can be done with an approximate formula,

$$n_k = \frac{2Qm_k}{NA_k v} \quad \text{for } k = 1, \ldots, 100, \tag{12}$$

where n_k is the gas density near the kth element with surface A_k corresponding an injected flux Q, v is the mean molecular velocity, other parameters are from Monte Carlo calculations: N is a number of generated test particles and m_k is a number of particles passed through the kth element. The approximate nature originates from uncertainty in the molecular velocity and its nonuniform field.

In the DPS1 model, the molecules that reached the entrance to TMP and were not pumped are included (as they were generated at this surface) in the gas density according to the following expression:

$$n_k = \frac{2Q}{Nv}\sum_{i=1}^{8}\left(f_i(1-\alpha_i)\frac{m_{k,i}}{A_k}\right) \quad \text{for } k = 1, \ldots, 100,$$

$$i = 1, \ldots, 8. \tag{13}$$

Here, index i corresponds to the results and parameters for the pumping surface i, and $m_{k,i}$ is a number of particles passed through the kth element when desorption in the TPMC modeling were from the ith pumping surface.

The test strips were set along the main axis of the DPS1 (two serial strips: 200 elements). The results of calculations with pump capture probability of 0.3 are shown by a green line on Fig. 7. The results are normalized to 1 at $x=4$ m (the entrance to the model).

The test facets were also set across the vacuum chamber (violet triangles on Fig. 7). These facets count particles arriving from one side only. Most of the facets were faces to the inlet and only two facets (with coordinates $x=5.37$ m and 7.53 m) were faces to the outlet. At the coordinate $x=5.37$ m, there were two test facets with different orienta-

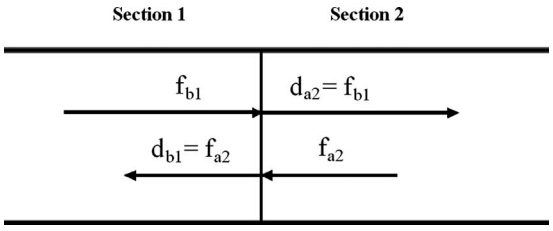


FIG. 8. Boundary conditions between two sections.

tion; one can clearly see that facets facing to the inlet give a 20% higher impingement rate than the one facing to the outlet. The impingement rate of the facets facing to the inlet is always higher than the one for the longitudinal one. This all indicates the molecular beaming effect.

Another interesting effect is that although there is only one source of gas at the inlet, the gas density profile shows a pronounced increase after each pumping port. This can be explained as such: some number of particles travel through the pumping port without collisions with its walls and collide with walls of the next tube; after that these particles can diffuse to either end.

IV. GAS FLOW-RATE REDUCTION FACTOR AND DENSITY RATIO OVER ENTIRE TRANSPORT LINE

Consider three serial sections with entrances a_1, a_2, and a_3 and exits b_1, b_2, and b_3. When it is necessary to model the density and gas flow rate, the boundary conditions are defined by the following gas flow balance (in dimensionless form, related to the overall inlet gas flow):

$$Q(a_1)=1, \quad Q(a_2)=-Q(b_1), \quad Q(a_3)=-Q(b_2). \tag{14}$$

For continuity reasons, the condition $Q(a_2)=-Q(b_1)$ is fulfilled when $d_{a2}=f_{b1}$ and $d_{b1}=f_{a2}$ (see Fig. 8), where f is a gas flux to the surface and d is the desorption flux from the surface (in the same terms as used for analysis in Ref. 11). Section 2 can be characterized by its capture probability, which is defined as

$$\chi_{\text{Sec 2}}=1-\frac{f_{a2}}{d_{a2}}=1-\frac{f_{a2}}{f_{b1}}. \tag{15}$$

Then, the flow d_{b1} from section 2 to section 1 is equal to

$$d_{b1}=f_{a2}=(1-\chi_{\text{Sec 2}})f_{b1}. \tag{16}$$

This illustrates that the results for the downstream section 2 are needed to model the upstream section 1 for obtaining section 2 capture probability.

This method is correct in assuming that the velocity field is the same on either side of the boundary between two sections. The TPMC code used for this work generates a cosine-law molecular distribution of desorbed molecules. However, in practice, the molecular distribution might be different for the molecules hitting the boundary between two sections from another side. This introduces the deviation of the results. To study how strong such a deviation could be, a separate TPMC model was built by splitting the DPS1-F in two halves. Comparing the results of this modeling to one for a full DPS1-F model has shown that the difference between two models is insignificant (less than 2%).

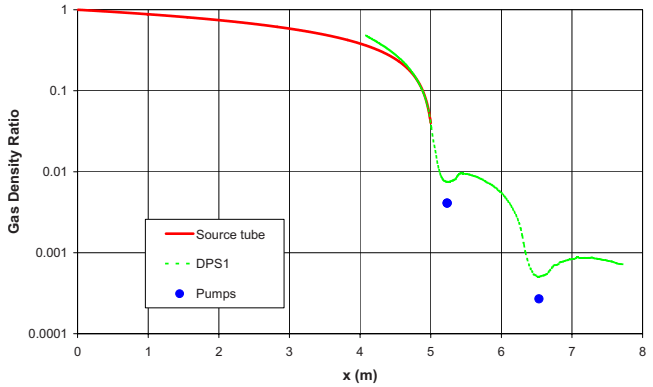


FIG. 9. (Color online) Merging solutions for WGTS tube and the complete DPS.

A. Merging the results for the WGTS tube and DPS1-F

It is necessary to mention here that including the 1 m long part of the WGTS tube in the DPS1 model plays a very important role in the model. The molecular velocity distribution formed during passing this 1 m tube builds up a molecular beam that goes directly to the exit without any collisions with the walls. The number of these molecules is significant. The model without the 1 m long tubular part of the WGTS gives a flow-rate reduction factor of about 600 against about 300 in the case with such a tube, i.e., it underestimates the molecular beaming effect by a factor of 2. If the molecular flow regime was everywhere along WGTS and DPS, the model must be built from the middle of the WGTS and the molecular beaming effect would be even stronger. Meanwhile, it should be noted that the gas flow regime is viscous in the middle and transitional at the end of WGTS; therefore, the number of intermolecular collisions grows toward the center of WGTS, and the beaming effect is diminished.

The conditions to find the correct point of joining two solutions for WGTS tube and DPS1 were as follows:

$$Q_{\text{WGTS}}(x_1)=Q_{\text{DPS1-F}}(x_1), \tag{17}$$

$$n_{\text{WGTS}}(x_1)=n_{\text{DPS1-F}}(x_1), \tag{18}$$

$$\frac{dn_{\text{WGTS}}(x_1)}{dx}=\frac{dn_{\text{DPS1-F}}(x_1)}{dx}. \tag{19}$$

In both models for the WGTS tube and DPS1, Q is sufficient to find by $n(x)$ and (dn/dx), conditions (18) and (19) are important to check that there is an overlapping interval where two solutions match each other. If the center of the WGTS corresponds to $x=0$, then the entrance to the DPS1-F model is at $x=4$ m. It was found that condition (17) is fulfilled for the source calculation with $P_{\text{ex}}/P_{\text{in}}=0.04$ at the interval 4.7 m $<x_1<5$ m, as shown in Fig. 9.

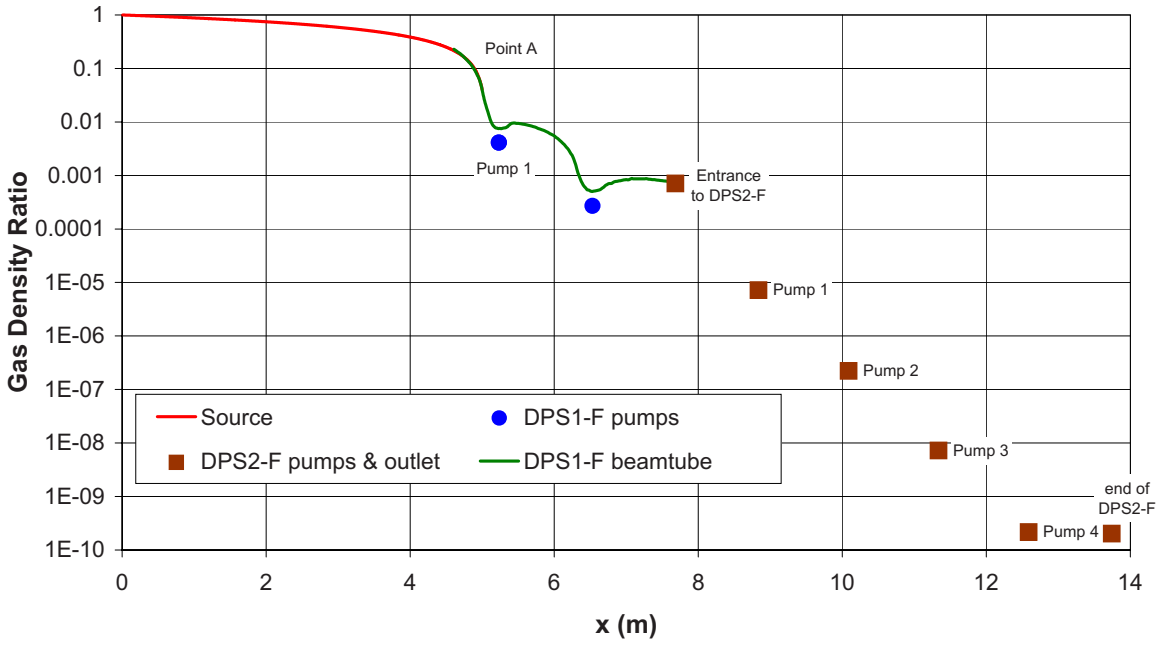


FIG. 10. (Color online) Gas density ratio for the complete differential pumping system (values for DPS2-F from Ref. 4).

B. Merging results for the DPS1-F and DPS2-F

The entrance boundary conditions for DPS2-F are

$$Q_{\mathrm{DPS1\text{-}F}}(\mathrm{outlet}) = Q_{\mathrm{DPS2\text{-}F}}(\mathrm{inlet}),$$

$$n_{\mathrm{DPS1\text{-}F}}(\mathrm{outlet}) = n_{\mathrm{DPS2\text{-}F}}(\mathrm{inlet}). \quad (20)$$

Now, it is possible to plot the flow-rate reduction factor and the gas density ratio along the transport line. The result for the flow rate and the gas density ratios are shown in Figs. 10 and 11 or the turbopump capture probability $\alpha=0.3$, which was estimated in Ref. 11. The overall gas density ratio along WGTS, DPS1-F, and DPS2-F is $R=2.0\times10^{-10}$ and the gas flow-rate reduction factor is $K=1.4\times10^{-8}$. The most important conclusion from these results is that the requirement to have a flow-rate reduction factor of 1.4×10^{-8} can be met. However, one must keep in mind that there is transitional flow around the first pumping port of DPS1, which means that the flow-rate reduction factors calculated with the TPMC method may not be very accurate. Moreover, there is the influence of temperature gradients so we must conclude that there is no safety margin included in the design of DPS1 and DPS2 with respect to the flow-rate reduction. Consequently, the design of the downstream sections of the transport system must account for the additional contingency needed. This will be discussed in detail in Sec. V.

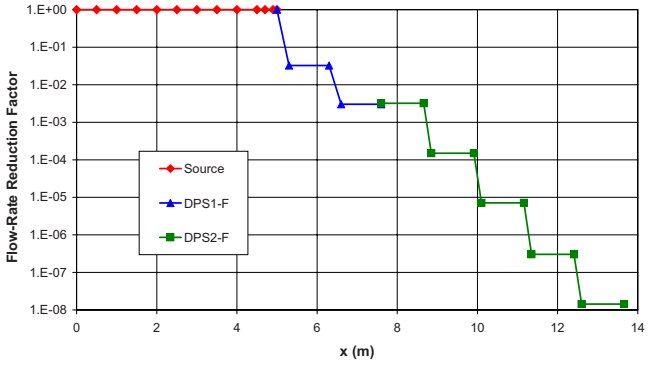


FIG. 11. (Color online) Flow-rate reduction factor for the complete differential pumping system.

V. REQUIREMENTS FOR THE REMAINING DOWNSTREAM TRANSPORT SYSTEM

As it was explained at the beginning of this article, the required flow-rate reduction factor K from source to spectrometer inlet is approximately 10^{-14}. The flow-rate reduction factor from source to the outlet of DPS2F is $K_{\mathrm{DPS1+DPS2}}=1.4\times10^{-8}$. Therefore, the remaining part of the transport system comprising the CPS and the prespectrometer (PS) should provide a minimum additional flow-rate reduction factor of about 7×10^{-7}. It is also preferable to have some safety margin: 1/30 for an accident with one failed TMP and about a factor $\frac{1}{2}$ for some differences between the model and a real design; hence, there is a need of $K_{\mathrm{CPS+PS}}\approx10^{-8}$.

VI. CONCLUSIONS

Numerical model results for the WGTS tube and the TPMC model results for DPS1-F are presented. It was shown that the strong molecular beaming effect limits the DPS1-F gas flow-rate reduction factor to $K_I\approx3\times10^{-3}$. These results were analyzed together with results published earlier for another part of KATRIN: DPS2-F. The calculated gas density ratio along WGTS tube, DPS1-F, and DPS2-F is $R=2.0\times10^{-10}$ and the gas flow-rate reduction factor is $K=1.4$

$\times 10^{-8}$. The remaining part of the transport system comprising CPS and PS should provide an additional flow-rate reduction of 10^{-8}.

[1]KATRIN Collaboration, KATRIN: A next generation tritium beta decay experiment with sub-eV sensitivity for the electron neutrino mass, 2001, http://arxiv.org/archive/hep-ex/0109033.
[2]KATRIN Collaboration, Forschungszentrum Karlsruhe Scientific Report No. FZKA 7090, 2005, http://www-ik.fzk.de/katrin.
[3]R. Gehring, J. Bonn, B. Bornschein, B. Flatt, K. P. Jüngst, H. Neumann, A. Osipowicz, and J. Pitel, IEEE Trans. Appl. Supercond. **14**, 589 (2004).
[4]F. Sharipov and V. Seleznev, J. Vac. Sci. Technol. A **12**, 2933 (1994).
[5]F. Sharipov, J. Vac. Sci. Technol. A **15**, 2434 (1997).
[6]F. Sharipov, Eur. J. Mech. B/Fluids **22**, 145 (2003).
[7]M. J. Assael, S. Mixafendi, and W. A. Wakeham, J. Phys. Chem. Ref. Data **15**, 1315 (1986).
[8]M. J. Assael, S. Mixafendi, and W. A. Wakeham, J. Phys. Chem. Ref. Data **16**, 189 (1987).
[9]J. M. J. Coremans, A. van Itterbeek, J. J. M. Beenakker, H. F. P. Knaap, and P. Zandbergen, Physica (Amsterdam) **24**, 557 (1958).
[10]F. Sharipov, Eur. J. Mech. B/Fluids **22**, 133 (2003).
[11]X. Luo, C. Day, V. Hauer, O. B. Malyshev, R. J. Reid, and F. Sharipov, Vacuum **80**, 864 (2006).
[12]MOLFLOW, R. Kersevan, ESRF, France, private communication.
[13]MOVAK3D, version 6.04, G. Class, Germany, private communication, 2004.